Determination of the Σ^+ Timelike Electromagnetic Form Factors

M. Ablikim *et al.**
(BESIII Collaboration)

(Received 1 August 2023; revised 24 November 2023; accepted 12 January 2024; published 22 February 2024)

Based on data samples collected with the BESIII detector at the BEPCII collider, the process $e^+e^- \to \Sigma^+\bar{\Sigma}^-$ is studied at center-of-mass energies $\sqrt{s} = 2.3960$, 2.6454, and 2.9000 GeV. Using a fully differential angular description of the final state particles, both the relative magnitude and phase information of the Σ^+ electromagnetic form factors in the timelike region are extracted. The relative phase between the electric and magnetic form factors is determined to be $\sin\Delta\Phi = -0.67 \pm 0.29(\mathrm{stat}) \pm 0.18(\mathrm{syst})$ at $\sqrt{s} = 2.3960$ GeV, $\Delta\Phi = 55° \pm 19°(\mathrm{stat}) \pm 14°(\mathrm{syst})$ at $\sqrt{s} = 2.6454$ GeV, and $78° \pm 22°(\mathrm{stat}) \pm 9°(\mathrm{syst})$ at $\sqrt{s} = 2.9000$ GeV. For the first time, the phase of the hyperon electromagnetic form factors is explored in a wide range of four-momentum transfer. The evolution of the phase along with four-momentum transfer is an important input for understanding its asymptotic behavior and the dynamics of baryons.

DOI: 10.1103/PhysRevLett.132.081904

Hyperons have a very similar quark composition to that of nucleons, except that one or more of the up or down quarks is replaced by strange quarks. Together with the nucleons, they form a spin-$1/2$ baryon octet under SU(3) symmetry [1,2]. As one of the fundamental physics observables of the baryons, electromagnetic form factors (EMFFs) provide a valuable perspective for understanding baryon structure [3–5] by probing internal charge and current distributions [6–9]. The EMFFs are analytic functions of the four-momentum transfer squared (q^2), and they can be divided into spacelike ($q^2 < 0$) and timelike ($q^2 > 0$) regions [10,11]. The former are often measured using electron-baryon elastic scattering experiments, while the latter use electron-positron annihilation into baryon antibaryon pairs or the reverse reaction. However, owing to the difficulties in producing stable and high-quality hyperon beams, it is challenging to study the EMFFs of hyperons in the spacelike region. Currently, only a few experiments have measured the EMFFs of hyperon in the spacelike region by elastic scattering of the hyperon beam off atomic electrons, and the range of $|q^2|$ for exploring EMFFs is limited due to kinematic constraints [12]. On the other hand, hyperons can be readily produced in electron-positron annihilation above their pair production thresholds. Therefore, the hyperon EMFFs are usually studied in the timelike region via $e^+e^- \to \gamma^* \to Y\bar{Y}$, where Y represents a hyperon with spin $1/2$, and these can be related to the spacelike region via dispersion relations [13].

A large number of measurements are available in the literature for the effective form factors (G_{eff}) of SU(3) baryons, which are extracted from production cross sections for $e^+e^- \to \gamma^* \to B\bar{B}$ under the assumption of the electric form factor ($|G_E|$) equal to the magnetic form factor ($|G_M|$) [14–29]. Previous measurements also exist for the modulus of EMFF ratios $|G_E/G_M|$, which are obtained by analyzing one-dimensional angular distributions [19,20,24,26]. However, according to the optical theorem, the form factors at the lowest order for the spacelike region are real due to the Hermiticity of the electromagnetic Hamiltonian, while in the timelike region they are complex [30,31]. Thus, a complete knowledge of EMFFs includes the relative phase $\Delta\Phi$ between electric and magnetic form factors, G_E and G_M. Since a nonzero $\Delta\Phi$ ensures a transverse polarization for the produced baryons [32], $\Delta\Phi$ can be extracted from the polarization. The transverse hyperon polarization is self-analyzed in their weak decays, while the polarization of nucleons needs additional dedicated devices to be measured.

The only previous determination of the $|G_E/G_M|$ and $\Delta\Phi$ for a baryon was performed at BESIII using the exclusive process $e^+e^- \to \Lambda\bar{\Lambda}$ at $\sqrt{s} = 2.396$ GeV. The relative phase of the Λ EMFFs was extracted by fitting the angular distributions [22]. Many theoretical activities [33–38] arose after this measurement. In Ref. [34], the EMFF ratio and their relative phase are also predicted for Σ hyperons, with a different dependence on the center-of-mass (c.m.) energy from the Λ case, reflecting complex dynamics. Though the G_{eff} and $|G_E/G_M|$ of the Σ hyperons have been measured by various experiments [26,29,39,40], the extraction of $\Delta\Phi$ for Σ is still unavailable. Thus, measurements of Σ EMFFs can

*Full author list given at the end of the Letter.

provide deeper insight into $\bar{Y}Y$ dynamics. Moreover, analyticity implies that the EMFFs tend to be real at large four-momentum transfer squared in the timelike region [35]. Since $\sin\Delta\Phi_\Lambda$ has previously been found to be significantly different from zero [22], this indicates that the asymptotic threshold has not yet been reached for the q^2 so far studied. The phase measurement in a broader four-momentum transfer squared range is thus important to ascertain the asymptotic behavior of the hyperons and to investigate its dynamical mechanisms [35].

In this Letter, we present a study of $e^+e^- \to \Sigma^+\bar{\Sigma}^-$ at three energy points, $\sqrt{s} = 2.3960$, 2.6454, and 2.9000 GeV, with a total integrated luminosity of 239.84 pb^{-1} collected with the Beijing Spectrometer (BESIII) at the Beijing Electron Positron Collider (BEPCII). The first energy point, 2.3960 GeV, is in close proximity to the production threshold for Σ^+ hyperon pairs ($2M_{\Sigma^+} = 2.3788$ GeV), where M_{Σ^+} represents the nominal mass of the Σ^+ [41]. Here 2.6454 GeV is a combined dataset of 2.6444 GeV and 2.6464 GeV. The $|G_E/G_M|$ ratio and the relative phase $\Delta\Phi$ are determined using a fully differential angular expression. The formalism is described in Ref. [42].

The description of the design and performance of the BESIII detector can be found in Ref. [43]. The Monte Carlo (MC) samples used to optimize event selection criteria are generated using a GEANT4-based [44] simulation software package. The CONEXC [45] generator is used to generate signal MC samples and includes higher order processes with one radiative photon in the final state. The input cross section of line shape for $e^+e^- \to \Sigma^+\bar{\Sigma}^-$ is obtained from Ref. [26]. The phase space (PHSP) model in EvtGen [46,47] is used to generate six million MC events to calculate the normalization factors in the multidimensional fits. The inclusive MC sample is generated with a HYBRID generator [48] for background analysis at each energy point.

Two different reconstruction methods are used to select $\Sigma^+\bar{\Sigma}^-$ pairs, according to the c.m. energy. At $\sqrt{s} = 2.3960$ GeV, due to the low tracking efficiency for low-momentum tracks, a single-tag method is used to select the process $e^+e^- \to \Sigma^+\bar{\Sigma}^- \to \bar{p}\pi^0 + X$, where X denotes inclusive decays of the Σ^+. At higher c.m. energies, both proton and antiproton are selected in the process $e^+e^- \to \Sigma^+\bar{\Sigma}^-$. To improve the detection efficiency, only one π^0 is reconstructed by two photons.

Charged tracks are reconstructed in the main drift chamber (MDC) as in Ref. [49]. Combined information of the specific ionization energy loss ($\mathrm{d}E/\mathrm{d}x$) in the MDC and the time of flight (TOF) is used to calculate particle identification (PID) probabilities for the pion, kaon, and proton hypotheses. The particle type with the highest probability is assigned for the track. At $\sqrt{s} = 2.3960$ GeV, only the $\mathrm{d}E/\mathrm{d}x$ is used for PID since the charged tracks cannot reach the TOF detector due to low momenta. Photon candidates are reconstructed from clusters of energy deposited in the electromagnetic calorimeter (EMC) as in Ref. [49]. To reject showers from charged tracks, the angle between the shower direction and the track extrapolated to the EMC must be greater than 20 degrees in the single-tag reconstruction.

In the single-tag reconstruction at $\sqrt{s} = 2.3960$ GeV, at least one good charged track, identified as an antiproton, is required. At least two good photons are required in each event. The $\bar{\Sigma}^-$ candidates are selected by looping over all possible $\bar{p}\gamma\gamma$ combinations. Two variables, ΔE and M_{bc}, which reflect energy and momentum conservation, are used to select $\bar{\Sigma}^-$ candidates. Here $\Delta E \equiv E - E_{\mathrm{beam}}$ is the energy difference, where E is the total measured energy of the $\bar{\Sigma}^-$ and E_{beam} is the beam energy, and $M_{\mathrm{bc}} \equiv \sqrt{E_{\mathrm{beam}}^2/c^4 - P_{\bar{\Sigma}^-}^2/c^2}$ is the beam-constrained mass and P is the magnitude of measured total momentum of the $\bar{\Sigma}^-$ candidate. Further selection criteria on the $\gamma\gamma$ invariant mass ($M_{\gamma\gamma}$) and ΔE, $0.126 < M_{\gamma\gamma} < 0.139$ GeV$/c^2$ and $-0.013 < \Delta E < 0.005$ GeV, are applied. After the above selections, the distribution of M_{bc} at $\sqrt{s} = 2.3960$ GeV is shown in Fig. 1(a).

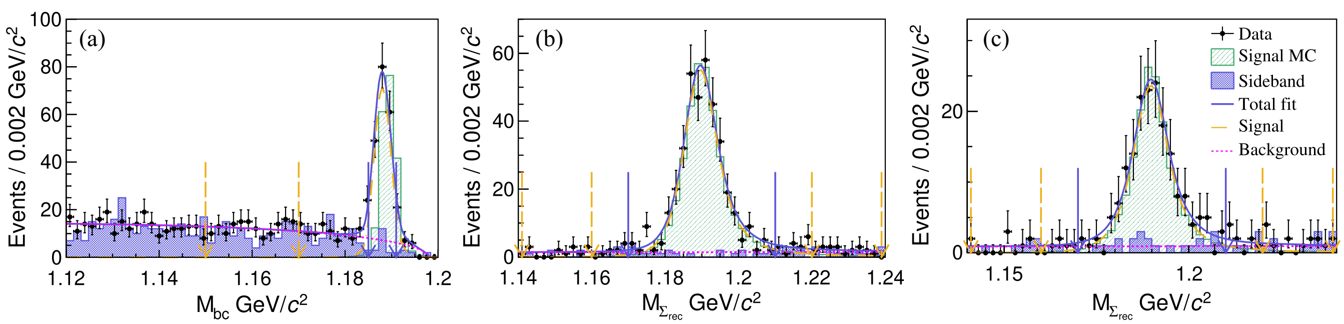

FIG. 1. The distributions of (a) M_{bc} at 2.3960 GeV, (b) $M_{\Sigma_{\mathrm{rec}}}$ at 2.6454 GeV, and (c) $M_{\Sigma_{\mathrm{rec}}}$ at 2.9000 GeV. The black dots with error bars are data. The histograms filled with green diagonal lines represent the signal MC samples, and the histograms filled with purple shading represent the backgrounds estimated by the sidebands. The purple solid lines are the total fit result. The yellow dash-dotted and magenta dotted lines are the signal and background shapes, respectively. The signal and background regions used for further angular analysis are indicated by purple solid-line arrows and yellow dashed-line arrows, respectively.

In the reconstruction with one missing π^0 at $\sqrt{s} = 2.6454$ and 2.9000 GeV, a good event must have at least two good charged tracks identified to be one proton and one antiproton. At least two good photons are selected, and π^0 candidates are reconstructed from pairs of photons as in Ref. [49]. At least one good π^0 candidate is required. To further remove potential background and improve the mass resolution, a two-constraint ($2C$) kinematic fit under the $e^+e^- \to p\bar{p}\pi^0\pi^0$ hypothesis is performed. The fit requires total energy-momentum conservation, and the $\gamma\gamma$ invariant mass is constrained to the nominal π^0 mass, while the other $\pi^0_{\rm miss}$ is treated as a missing particle with free three-momentum. For events with more than one $\pi^0_{\gamma\gamma}$ candidate, by looping over the $\pi^0_{\gamma\gamma}$ candidates in the kinematic fit, the best $\pi^0_{\gamma\gamma}$ is selected with the minimum χ^2_{2C} which is further required to be less than 15. The $\pi^0_{\gamma\gamma}$ is then paired with either the proton or antiproton depending on which combination gives the minimum $|M_{(p\pi^0_{\gamma\gamma}/\bar{p}\pi^0_{\gamma\gamma})} - M_{\Sigma^+}|$, and the best combination is denoted as $\Sigma_{\rm tag}$. The signal region in the invariant mass of $\Sigma_{\rm tag}$ is chosen as $1.175 < M_{\Sigma_{\rm tag}} < 1.200$ GeV$/c^2$. The recoiling mass spectrum against $\Sigma_{\rm tag}$, $M_{\Sigma_{\rm rec}}$, after the previously described selections, is shown in Figs. 1(b) and 1(c).

Both the inclusive MC sample and the data sideband are used to study the potential background events. The main background, found in the inclusive MC sample, includes processes from e^+e^- annihilation events with the same final states as the signal, with an additional photon, and with intermediate states like Λ, Σ, and Δ baryons. The background in the inclusive MC sample is smooth. The sideband regions are defined as $-0.040 < \Delta E < -0.031$ GeV and $0.028 < \Delta E < 0.037$ GeV for $\sqrt{s} = 2.3960$ GeV, and $1.135 < M_{\Sigma_{\rm tag}} < 1.150$ GeV$/c^2$ and $1.225 < M_{\Sigma_{\rm tag}} < 1.240$ GeV$/c^2$ for other energy points. As shown in Fig. 1, the backgrounds in the sideband regions in both $M_{\rm bc}$ and $M_{\Sigma_{\rm rec}}$ are smooth, so no further selection is applied.

To extract the signal yield, a simultaneous fit of $M_{\rm bc}$ and $M_{\Sigma_{\rm rec}}$ is applied. In the fit, the probability density functions (PDF) of signal events are described by MC-simulated shapes, extracted from the signal MC sample, convolved with a Gaussian function. The PDFs of background events are described by an Argus function [50] at $\sqrt{s} = 2.3960$ GeV and a linear function at $\sqrt{s} = 2.6454$ and 2.9000 GeV. The best fit results are shown in Fig. 1. The numbers of signal events are 207 ± 17, 364 ± 21, and 168 ± 15 at 2.3960, 2.6454, and 2.9000 GeV, respectively, and the corresponding MC selection efficiencies are 11.33%, 34.39%, and 33.58%, respectively. Furthermore, a cross-check of the Born cross section with the previous BESIII results [26] is performed to ensure the reliability of the selection method. To ensure a pure sample for the further angular distribution analysis, tighter selections are applied on both $M_{\rm bc}$ and $M_{\Sigma_{\rm rec}}$, requiring $1.185 < M_{\rm bc} < 1.191$ GeV$/c^2$ and $1.170 < M_{\Sigma_{\rm rec}} < 1.210$ GeV$/c^2$ as indicated with arrows in Fig. 1. The background fractions are 12.7%, 7.7%, and 10.2% at 2.3960, 2.6454, and 2.9000 GeV, respectively.

Following Refs. [42,51], the joint angular distribution $\mathcal{W}(\xi)$ of $e^+e^- \to \Sigma^+(\to p\pi^0)\bar{\Sigma}^-(\to \bar{p}\pi^0)$ can be expressed as

$$\mathcal{W}(\xi) \propto \mathcal{F}_0(\xi) + \alpha\mathcal{F}_5(\xi) + \alpha_1\alpha_2\Big[\mathcal{F}_1(\xi) + \sqrt{1-\alpha^2}\cos(\Delta\Phi)\mathcal{F}_2(\xi) + \alpha\mathcal{F}_6(\xi)\Big] + \sqrt{1-\alpha^2}\sin(\Delta\Phi)\big[-\alpha_1\mathcal{F}_3(\xi) + \alpha_2\mathcal{F}_4(\xi)\big], \quad (1)$$

where ξ is a five-dimensional vector, $\xi = (\theta_{\Sigma^+}, \theta_1, \theta_2, \phi_1, \phi_2)$; θ_{Σ^+} is the angle between the Σ^+ hyperon and positron beam; θ_1 (θ_2) and ϕ_1 (ϕ_2) are the polar and azimuthal angles of the proton (antiproton) with respect to the Σ^+ and $\bar{\Sigma}^-$ helicity frame, respectively; and α_1 and α_2 are the decay asymmetry parameters of the Σ^+ and $\bar{\Sigma}^-$. The set of angular distribution functions $\mathcal{F}_i(\xi)$ $(i = 0, 1, \ldots, 6)$ are obtained in Ref. [42]. Owing to limited statistics, we assume CP to be conserved and $\alpha_1 = -\alpha_2 = -0.980$ [41]. The α is the angular distribution parameter describing the ratio of the two helicity amplitudes in $e^+e^- \to \Sigma^+\bar{\Sigma}^-$, and $\Delta\Phi$ is their relative phase. The α relates to $|G_E/G_M|$ via [52]

$$|G_E/G_M| = \sqrt{\frac{s(1-\alpha)}{4M^2_{\Sigma^+}(1+\alpha)}}. \quad (2)$$

Since only one hyperon is reconstructed at $\sqrt{s} = 2.3960$ GeV, θ_1 and ϕ_1 are integrated at this energy point, and the angular distribution becomes

$$\mathcal{W}(\xi) \propto \mathcal{F}_0(\xi) + \alpha\mathcal{F}_5(\xi) + \sqrt{1-\alpha^2}\sin(\Delta\Phi)\alpha_2\mathcal{F}_4(\xi). \quad (3)$$

The parameters α and $\Delta\Phi$ can be extracted by a multidimensional maximum likelihood fit to data. The joint likelihood function for observing N events in the data sample is

$$\mathcal{L} = \prod_{i=1}^{N}\mathcal{P}(\xi_i;\alpha,\Delta\Phi) = \prod_{i=1}^{N}\mathcal{C}\mathcal{W}(\xi_i;\alpha,\Delta\Phi)\epsilon(\xi_i), \quad (4)$$

where $\mathcal{P}(\xi_i;\alpha,\Delta\Phi)$ is the probability density function of ξ_i, i is the corresponding event index, and $\epsilon(\xi_i)$ is the

TABLE I. Fit results for α, $\Delta\Phi(°)$, $\sin(\Delta\Phi)$, and $|G_E/G_M|$ at each energy point.

$\sqrt{s}$ (GeV)	2.3960	2.6454	2.9000
α	$-0.47 \pm 0.18 \pm 0.09$	$0.41 \pm 0.12 \pm 0.06$	$0.35 \pm 0.17 \pm 0.15$
$\Delta\Phi(°)$	$-42 \pm 22 \pm 14$ ($-138 \pm 22 \pm 14$)	$55 \pm 19 \pm 14$	$78 \pm 22 \pm 9$
$\sin\Delta\Phi$	$-0.67 \pm 0.29 \pm 0.18$		
$\|G_E/G_M\|$	$1.69 \pm 0.38 \pm 0.20$	$0.72 \pm 0.11 \pm 0.06$	$0.85 \pm 0.16 \pm 0.15$

efficiency of each event. The normalization factor $\mathcal{C}$ is given by $\mathcal{C}^{-1} = \int \mathcal{W}(\xi; \alpha, \Delta\Phi)\epsilon(\xi)d\xi$ and evaluated by the PHSP signal MC sample. The parameters α and $\Delta\Phi$ are extracted by minimizing the likelihood function

$$S = -\ln \mathcal{L}_{\text{Data}} + \ln \mathcal{L}_{\text{Bkg}}, \tag{5}$$

where $\mathcal{L}_{\text{Data}}$ is the corresponding likelihood value of data and $\mathcal{L}_{\text{Bkg}}$ represents the background, estimated with data events in the background region indicated in Fig. 1 and normalized to the signal region. The best fit results for α, $\Delta\Phi$, and (or) $\sin(\Delta\Phi)$ are summarized in Table I, where only $\sin(\Delta\Phi)$ can be extracted at 2.3960 GeV due to the application of a single-tag method and the lack of sufficient angular distribution information.

Furthermore, the nonzero $\Delta\Phi$ will lead to a dependence of the polarization on the scattering angle of the Σ^+ [32,51]:

$$P_y = -\frac{\sqrt{1-\alpha^2}\sin\theta_{\Sigma^+}\cos\theta_{\Sigma^+}}{1+\alpha\cos^2\theta_{\Sigma^+}}\sin(\Delta\Phi). \tag{6}$$

Experimentally, the P_y is determined by

$$P_y = \frac{m}{N}\sum_{i=1}^{N_k}\frac{(3+\alpha)(n_{1,y}^i + n_{2,y}^i)}{(\alpha_1-\alpha_2)(1+\alpha\cos^2\theta_{\Sigma^+}^i)}, \tag{7}$$

where N is the total number of events in the dataset and $m = 8$ is the number of bins in $\cos\theta_{\Sigma^+}$; N_k denotes the number of events in the kth $\cos\theta_{\Sigma^+}$ bin; and $n_{1,y}$ ($n_{2,y}$) is the projection of a proton (antiproton) perpendicular to the scattering plane in the rest frame of Σ^+ ($\bar{\Sigma}^-$). To test the goodness of the fit results, the signal MC sample is generated using Eqs. (1) and (3) and inputting the measured parameters from the data. The angular-dependent transverse polarization of Σ is obtained as shown in Fig. 2.

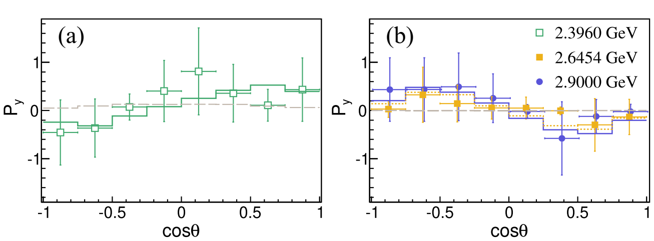

FIG. 2. The polarization P_y as a function of the scattering angle at 2.3960 GeV (a) and 2.6454 and 2.9000 GeV (b). The open squares, solid squares, and dots are data. The histograms with solid lines (dotted line at 2.6454 GeV) are signal MC samples based on the fit results, and the histograms with the gray dashed lines are the PHSP signal MC samples at each energy point.

The sources of systematic uncertainties are summarized in Table II. For the first four sources in Table II, uncertainties are caused by the event selection and are evaluated by varying the selection criteria. For the fifth to eighth sources in Table II, the uncertainties from the fit procedure are estimated with alternative fits by varying the signal region, changing the sideband selections, and varying the fixed decay parameters (α_1, α_2) by $\pm 1\sigma$, individually. The maximum difference with the nominal value is taken as the uncertainty. To estimate the systematic uncertainty of the fit method, 500 sets of signal MC samples with the parameters from Table I are generated and fitted to obtain the distribution of the output parameters, and the difference between the input and averaged output values is assigned as the systematic uncertainty. Some inconsistencies between the data and MC simulation are observed in the M_{bc} distribution, as shown in Fig. 1(a). To estimate their effect on the final results, the measurement of beam energy and the calibration of the $\bar{\Sigma}^-$ momentum are investigated. For the E_{beam} calibration, we generate three MC samples with

TABLE II. The systematic uncertainties for α, $\Delta\Phi(°)$, and $\sin(\Delta\Phi)$ at each energy point (in GeV).

	2.3960		2.6454		2.9000	
Source	α	$\sin(\Delta\Phi)$	α	$\Delta\Phi$	α	$\Delta\Phi$
ΔE cut	0.03	0.02				
$\gamma\gamma$ mass window	0.04	0.06				
χ^2_{2C} cut			0.04	5	0.08	5
Σ_{tag} mass window			0.00	3	0.06	2
Signal region	0.05	0.16	0.04	9	0.05	4
Sideband region	0.02	0.06	0.02	9	0.09	5
α_1			0.01	0	0.00	1
α_2	0.00	0.01	0.01	0	0.00	1
Fit method	0.00	0.01	0.02	2	0.03	2
E_{beam} calibration	0.03	0.00				
Momentum calibration	0.04	0.01				
Total	0.09	0.18	0.06	14	0.15	9

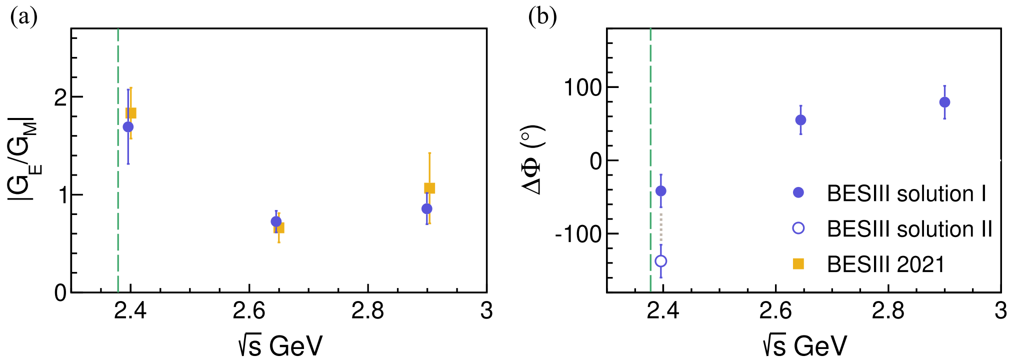

FIG. 3. Results for $|G_E/G_M|$ (a) and the relative phase $\Delta\Phi$ (b) from this work (purple dots). The yellow squares in (a) denote the previous results from BESIII [26]. The open circle in (b) represents the second solution of $\Delta\Phi$ at 2.3960 GeV. The vertical dashed lines indicate the production threshold for $e^+e^- \to \Sigma^+\bar{\Sigma}^-$, where $|G_E/G_M| = 1$ and $\Delta\Phi = 0°$ by definition.

different c.m. energies, defined around 2.3960 GeV in steps of 1 MeV, that is, 2.3950, 2.3970, and 2.3980 GeV, and choose the one that gives the best description of the data in the fit procedure. For the $\bar{\Sigma}^-$ momentum calibration, ten MC samples are generated, with different scale factors for the three-momentum of antiproton in each sample. The scale factors are defined in steps of 0.001 from 1.040 to 1.049, and we choose the one giving the best description of the data in the fit procedure. The differences between the updated and nominal results are taken as the systematic uncertainties. In Table II, the individual uncertainties are assumed to be uncorrelated and are added in quadrature.

In summary, the process $e^+e^- \to \Sigma^+\bar{\Sigma}^-$ is studied at 2.3960, 2.6454, and 2.9000 GeV. Using a joint angular distribution analysis, the final results for $|G_E/G_M|$, the relative phase $\Delta\Phi$, and $\sin\Delta\Phi$ are summarized in Table I and plotted in Fig. 3, where the relative phase of the Σ^+ hyperon is measured for the first time in a wide four-momentum transfer range.

The precision of $|G_E/G_M|$ is improved compared with the previous measurement [26] at 2.6454 and 2.9000 GeV. Since only the sine value of $\Delta\Phi$ can be extracted at 2.3960 GeV, the two solutions are plotted as shown in Fig. 3(b), and there is a significant discrepancy between our experimental result for $\Delta\Phi$ and the theoretical predictions from the $\bar{Y}Y$ potential model [34]. On the other hand, in Fig. 3(b), $\Delta\Phi$ is less than zero at 2.3960 GeV and greater than zero at 2.6454 GeV, which implies that there may be at least one $\Delta\Phi = 0°$ between these two energy points. Such an evolution will be important input for understanding its asymptotic behavior [35] and the dynamics of baryons. Moreover, the fact that the relative phase is still increasing at 2.9000 GeV indicates that the asymptotic threshold has not yet been reached.

The authors thank Professor L. Y. Dai for the helpful discussion. The BESIII Collaboration thanks the staff of BEPCII and the IHEP computing center and the supercomputing center of USTC for their strong support. This work is supported in part by National Key R&D Program of China under Contracts No. 2020YFA0406400, No. 2020YFA0406300, and No. 2023YFA1609400; National Natural Science Foundation of China (NSFC) under Contracts No. 11905092, No. 12105132, No. 11705078, No. 11625523, No. 12105276, No. 12122509, No. 11635010, No. 11735014, No. 11835012, No. 11935015, No. 11935016, No. 11935018, No. 11961141012, No. 12022510, No. 12025502, No. 12035009, No. 12035013, No. 12061131003, No. 12192260, No. 12192261, No. 12192262, No. 12192263, No. 12192264, No. 12192265, No. 12221005, No. 12225509, and No. 12235017; the Chinese Academy of Sciences (CAS) Large-Scale Scientific Facility Program; the CAS Center for Excellence in Particle Physics (CCEPP); Joint Large-Scale Scientific Facility Funds of the NSFC and CAS under Contracts No. U1732263, No. U1832103, No. U1832207, and No. U2032111; CAS Key Research Program of Frontier Sciences under Contracts No. QYZDJ-SSW-SLH003 and No. QYZDJ-SSW-SLH040; 100 Talents Program of CAS; The Institute of Nuclear and Particle Physics (INPAC) and Shanghai Key Laboratory for Particle Physics and Cosmology; The Double First-Class university project foundation of USTC; ERC under Contract No. 758462; European Union's Horizon 2020 research and innovation programme under Marie Sklodowska-Curie Grant Agreement under Contract No. 894790; German Research Foundation DFG under Contracts No. 455635585, Collaborative Research Center CRC 1044, FOR5327, GRK 2149; Istituto Nazionale di Fisica Nucleare, Italy; Ministry of Development of Turkey under Contract No. DPT2006K-120470; National Research Foundation of Korea under Contract No. NRF-2022R1A2C1092335; National Science and Technology fund of Mongolia; National Science Research and Innovation Fund (NSRF) via the Program Management

Unit for Human Resources & Institutional Development, Research and Innovation of Thailand under Contract No. B16F640076; Polish National Science Centre under Contract No. 2019/35/O/ST2/02907; The Swedish Research Council; U.S. Department of Energy under Contract No. DE-FG02-05ER41374; The PhD Start-up Fund of Natural Science Foundation of Liaoning Province of China under Contract No. 2019-BS-113; Education Department of Liaoning Province Scientific research Foundation of Liaoning Provincial Department of Education under Contract No. LQN201902; Foundation of Innovation team 2020, Liaoning Province; Opening Foundation of Songshan Lake Materials Laboratory, Grant No. 2021SLABFK04. CAS Youth Team Program under Contract No. YSBR-101. Knut & Alice Wallenberg Foundation, Contract No. 2021.0174 and No. 2021.0299; Swedish Research Council, Contract No. 2019.04594; The Swedish Foundation for International Cooperation in Research and Higher Education, CH2018-7756.

[1] M. Gell-Mann, Phys. Lett. **8**, 214 (1964).
[2] G. Zweig, Report No. CERN-TH-401, 1964, https://cds.cern.ch/record/352337.
[3] J. C. Bernauer *et al.* (A1 Collaboration), Phys. Rev. Lett. **105**, 242001 (2010).
[4] G. Ramalho, K. Tsushima, and A. W. Thomas, J. Phys. G **40**, 015102 (2013).
[5] G. Eichmann, H. Sanchis-Alepuz, R. Williams, R. Alkofer, and C. S. Fischer, Prog. Part. Nucl. Phys. **91**, 1 (2016).
[6] R. Hofstadter, Rev. Mod. Phys. **28**, 214 (1956).
[7] S. J. Brodsky and G. R. Farrar, Phys. Rev. D **11**, 1309 (1975).
[8] L. S. Geng, J. Martin Camalich, L. Alvarez-Ruso, and M. J. Vicente Vacas, Phys. Rev. Lett. **101**, 222002 (2008).
[9] J. R. Green, J. W. Negele, A. V. Pochinsky, S. N. Syritsyn, M. Engelhardt, and S. Krieg, Phys. Rev. D **90**, 074507 (2014).
[10] N. Cabibbo and R. Gatto, Phys. Rev. **124**, 1577 (1961).
[11] V. Punjabi, C. F. Perdrisat, M. K. Jones, E. J. Brash, and C. E. Carlson, Eur. Phys. J. A **51**, 79 (2015).
[12] I. M. Gough Eschrich *et al.* (SELEX Collaboration), Phys. Lett. B **522**, 233 (2001).
[13] H. Pfister, Z. Phys. **211**, 176 (1968).
[14] D. Bisello *et al.*, Nucl. Phys. **B224**, 379 (1983).
[15] D. Bisello *et al.* (DM2 Collaboration), Z. Phys. C **48**, 23 (1990).
[16] A. Antonelli *et al.*, Nucl. Phys. **B517**, 3 (1998).
[17] M. Ablikim *et al.* (BES Collaboration), Phys. Lett. B **630**, 14 (2005).
[18] M. N. Achasov *et al.*, Phys. Rev. D **90**, 112007 (2014).
[19] M. Ablikim *et al.* (BESIII Collaboration), Phys. Rev. D **91**, 112004 (2015).
[20] R. R. Akhmetshin *et al.* (CMD-3 Collaboration), Phys. Lett. B **759**, 634 (2016).
[21] M. Ablikim *et al.* (BESIII Collaboration), Phys. Rev. D **97**, 032013 (2018).
[22] M. Ablikim *et al.* (BESIII Collaboration), Phys. Rev. Lett. **123**, 122003 (2019).
[23] M. Ablikim *et al.* (BESIII Collaboration), Phys. Rev. Lett. **124**, 032002 (2020).
[24] M. Ablikim *et al.* (BESIII Collaboration), Phys. Rev. Lett. **124**, 042001 (2020).
[25] M. Ablikim *et al.* (BESIII Collaboration), Phys. Rev. D **103**, 012005 (2021).
[26] M. Ablikim *et al.* (BESIII Collaboration), Phys. Lett. B **814**, 136110 (2021).
[27] M. Ablikim *et al.* (BESIII Collaboration), Phys. Lett. B **820**, 136557 (2021).
[28] M. Ablikim *et al.* (BESIII Collaboration), Nat. Phys. **17**, 1200 (2021).
[29] M. Ablikim *et al.* (BESIII Collaboration), Phys. Lett. B **831**, 137187 (2022).
[30] E. Tomasi-Gustafsson, F. Lacroix, C. Duterte, and G. I. Gakh, Eur. Phys. J. A **24**, 419 (2005).
[31] A. Denig and G. Salme, Prog. Part. Nucl. Phys. **68**, 113 (2013).
[32] A. Z. Dubnickova, S. Dubnicka, and M. P. Rekalo, Nuovo Cimento Soc. Ital. Fis. **109A**, 241 (1996).
[33] Y. L. Yang, D. Y. Chen, and Z. Lu, Phys. Rev. D **100**, 073007 (2019).
[34] J. Haidenbauer, U.-G. Meißner, and L. Y. Dai, Phys. Rev. D **103**, 014028 (2021).
[35] A. Mangoni, S. Pacetti, and E. Tomasi-Gustafsson, Phys. Rev. D **104**, 116016 (2021).
[36] A. X. Dai, Z. Y. Li, L. Chang, and J. J. Xie, Chin. Phys. C **46**, 073104 (2022).
[37] Y. H. Lin, H. W. Hammer, and U.-G. Meißner, Eur. Phys. J. C **82**, 1091 (2022).
[38] Z. Y. Li, A. X. Dai, and J. J. Xie, Chin. Phys. Lett. **39**, 011201 (2022).
[39] B. Aubert *et al.* (*BABAR* Collaboration), Phys. Rev. D **76**, 092006 (2007).
[40] G. Gong *et al.* (Belle Collaboration), Phys. Rev. D **107**, 072008 (2023).
[41] R. L. Workman *et al.* (Particle Data Group), Prog. Theor. Exp. Phys. **2022**, 083C01 (2022).
[42] E. Perotti, G. Fäldt, A. Kupsc, S. Leupold, and J. J. Song, Phys. Rev. D **99**, 056008 (2019).
[43] M. Ablikim *et al.* (BESIII Collaboration), Nucl. Instrum. Methods Phys. Res., Sect. A **614**, 345 (2010).
[44] S. Agostinelli *et al.* (GEANT4 Collaboration), Nucl. Instrum. Methods Phys. Res., Sect. A **506**, 250 (2003).
[45] R. G. Ping, Chin. Phys. C **38**, 083001 (2014).
[46] D. J. Lange, Nucl. Instrum. Methods Phys. Res., Sect. A **462**, 152 (2001).
[47] R. G. Ping, Chin. Phys. C **32**, 599 (2008).
[48] R. G. Ping *et al.*, Chin. Phys. C **40**, 113002 (2016).
[49] M. Ablikim *et al.* (BESIII Collaboration), Phys. Rev. Lett. **125**, 052004 (2020).
[50] H. Albrecht *et al.* (ARGUS Collaboration), Phys. Lett. B **241**, 278 (1990).
[51] G. Fäldt and A. Kupsc, Phys. Lett. B **772**, 16 (2017).
[52] S. Pacetti, R. Baldini Ferroli, and E. Tomasi-Gustafsson, Phys. Rep. **550**, 1 (2015).

M. Ablikim,[1] M. N. Achasov,[5,b] P. Adlarson,[75] X. C. Ai,[81] R. Aliberti,[36] A. Amoroso,[74a,74c] M. R. An,[40] Q. An,[71,58] Y. Bai,[57] O. Bakina,[37] I. Balossino,[30a] Y. Ban,[47,g] V. Batozskaya,[1,45] K. Begzsuren,[33] N. Berger,[36] M. Berlowski,[45] M. Bertani,[29a] D. Bettoni,[30a] F. Bianchi,[74a,74c] E. Bianco,[74a,74c] A. Bortone,[74a,74c] I. Boyko,[37] R. A. Briere,[6] A. Brueggemann,[68] H. Cai,[76] X. Cai,[1,58] A. Calcaterra,[29a] G. F. Cao,[1,63] N. Cao,[1,63] S. A. Cetin,[62a] J. F. Chang,[1,58] T. T. Chang,[77] W. L. Chang,[1,63] G. R. Che,[44] G. Chelkov,[37,a] C. Chen,[44] Chao Chen,[55] G. Chen,[1] H. S. Chen,[1,63] M. L. Chen,[1,58,63] S. J. Chen,[43] S. M. Chen,[61] T. Chen,[1,63] X. R. Chen,[32,63] X. T. Chen,[1,63] Y. B. Chen,[1,58] Y. Q. Chen,[35] Z. J. Chen,[26,h] W. S. Cheng,[74c] S. K. Choi,[11] X. Chu,[44] G. Cibinetto,[30a] S. C. Coen,[4] F. Cossio,[74c] J. J. Cui,[50] H. L. Dai,[1,58] J. P. Dai,[79] A. Dbeyssi,[19] R. E. de Boer,[4] D. Dedovich,[37] Z. Y. Deng,[1] A. Denig,[36] I. Denysenko,[37] M. Destefanis,[74a,74c] F. De Mori,[74a,74c] B. Ding,[66,1] X. X. Ding,[47,g] Y. Ding,[41] Y. Ding,[35] J. Dong,[1,58] L. Y. Dong,[1,63] M. Y. Dong,[1,58,63] X. Dong,[76] M. C. Du,[1] S. X. Du,[81] Z. H. Duan,[43] P. Egorov,[37,a] Y. H. Y. Fan,[46] Y. L. Fan,[76] J. Fang,[1,58] S. S. Fang,[1,63] W. X. Fang,[1] Y. Fang,[1] R. Farinelli,[30a] L. Fava,[74b,74c] F. Feldbauer,[4] G. Felici,[29a] C. Q. Feng,[71,58] J. H. Feng,[59] K. Fischer,[69] M. Fritsch,[4] C. Fritzsch,[68] C. D. Fu,[1] J. L. Fu,[63] Y. W. Fu,[1] H. Gao,[63] Y. N. Gao,[47,g] Yang Gao,[71,58] S. Garbolino,[74c] I. Garzia,[30a,30b] P. T. Ge,[76] Z. W. Ge,[43] C. Geng,[59] E. M. Gersabeck,[67] A. Gilman,[69] K. Goetzen,[14] L. Gong,[41] W. X. Gong,[1,58] W. Gradl,[36] S. Gramigna,[30a,30b] M. Greco,[74a,74c] M. H. Gu,[1,58] Y. T. Gu,[16] C. Y. Guan,[1,63] Z. L. Guan,[23] A. Q. Guo,[32,63] L. B. Guo,[42] M. J. Guo,[50] R. P. Guo,[49] Y. P. Guo,[13,f] A. Guskov,[37,a] T. T. Han,[50] W. Y. Han,[40] X. Q. Hao,[20] F. A. Harris,[65] K. K. He,[55] K. L. He,[1,63] F. H. H. Heinsius,[4] C. H. Heinz,[36] Y. K. Heng,[1,58,63] C. Herold,[60] T. Holtmann,[4] P. C. Hong,[13,f] G. Y. Hou,[1,63] X. T. Hou,[1,63] Y. R. Hou,[63] Z. L. Hou,[1] H. M. Hu,[1,63] J. F. Hu,[56,i] T. Hu,[1,58,63] Y. Hu,[1] G. S. Huang,[71,58] K. X. Huang,[59] L. Q. Huang,[32,63] X. T. Huang,[50] Y. P. Huang,[1] T. Hussain,[73] N. Hüsken,[28,36] W. Imoehl,[28] N. in der Wiesche,[68] J. Jackson,[28] S. Jaeger,[4] S. Janchiv,[33] J. H. Jeong,[11] Q. Ji,[1] Q. P. Ji,[20] X. B. Ji,[1,63] X. L. Ji,[1,58] Y. Y. Ji,[50] X. Q. Jia,[50] Z. K. Jia,[71,58] H. J. Jiang,[76] P. C. Jiang,[47,g] S. S. Jiang,[40] T. J. Jiang,[17] X. S. Jiang,[1,58,63] Y. Jiang,[63] J. B. Jiao,[50] Z. Jiao,[24] S. Jin,[43] Y. Jin,[66] M. Q. Jing,[1,63] T. Johansson,[75] X. K.,[1] S. Kabana,[34] N. Kalantar-Nayestanaki,[64] X. L. Kang,[10] X. S. Kang,[41] M. Kavatsyuk,[64] B. C. Ke,[81] A. Khoukaz,[68] R. Kiuchi,[1] R. Kliemt,[14] O. B. Kolcu,[62a] B. Kopf,[4] M. Kuessner,[4] A. Kupsc,[45,75] W. Kühn,[38] J. J. Lane,[67] P. Larin,[19] A. Lavania,[27] L. Lavezzi,[74a,74c] T. T. Lei,[71,58] Z. H. Lei,[71,58] H. Leithoff,[36] M. Lellmann,[36] T. Lenz,[36] C. Li,[44] C. Li,[48] C. H. Li,[40] Cheng Li,[71,58] D. M. Li,[81] F. Li,[1,58] G. Li,[1] H. Li,[71,58] H. B. Li,[1,63] H. J. Li,[20] H. N. Li,[56,i] Hui Li,[44] J. R. Li,[61] J. S. Li,[59] J. W. Li,[50] K. L. Li,[20] Ke Li,[1] L. J. Li,[1,63] L. K. Li,[1] Lei Li,[3] M. H. Li,[44] P. R. Li,[39,j,k] Q. X. Li,[50] S. X. Li,[13] T. Li,[50] W. D. Li,[1,63] W. G. Li,[1] X. H. Li,[71,58] X. L. Li,[50] Xiaoyu Li,[1,63] Y. G. Li,[47,g] Z. J. Li,[59] Z. X. Li,[16] C. Liang,[43] H. Liang,[1,63] H. Liang,[35] H. Liang,[71,58] Y. F. Liang,[54] Y. T. Liang,[32,63] G. R. Liao,[15] L. Z. Liao,[50] Y. P. Liao,[1,63] J. Libby,[27] A. Limphirat,[60] D. X. Lin,[32,63] T. Lin,[1] B. J. Liu,[1] B. X. Liu,[76] C. Liu,[35] C. X. Liu,[1] F. H. Liu,[53] Fang Liu,[1] Feng Liu,[7] G. M. Liu,[56,i] H. Liu,[39,j,k] H. B. Liu,[16] H. M. Liu,[1,63] Huanhuan Liu,[1] Huihui Liu,[22] J. B. Liu,[71,58] J. L. Liu,[72] J. Y. Liu,[1,63] K. Liu,[1] K. Y. Liu,[41] Ke Liu,[23] L. Liu,[71,58] L. C. Liu,[44] Lu Liu,[44] M. H. Liu,[13,f] P. L. Liu,[1] Q. Liu,[63] S. B. Liu,[71,58] T. Liu,[13,f] W. K. Liu,[44] W. M. Liu,[71,58] X. Liu,[39,j,k] Y. Liu,[81] Y. Liu,[39,j,k] Y. B. Liu,[44] Z. A. Liu,[1,58,63] Z. Q. Liu,[50] X. C. Lou,[1,58,63] F. X. Lu,[59] H. J. Lu,[24] J. G. Lu,[1,58] X. L. Lu,[1] Y. Lu,[8] Y. P. Lu,[1,58] Z. H. Lu,[1,63] C. L. Luo,[42] M. X. Luo,[80] T. Luo,[13,f] X. L. Luo,[1,58] X. R. Lyu,[63] Y. F. Lyu,[44] F. C. Ma,[41] H. L. Ma,[1] J. L. Ma,[1,63] L. L. Ma,[50] M. M. Ma,[1,63] Q. M. Ma,[1] R. Q. Ma,[1,63] R. T. Ma,[63] X. Y. Ma,[1,58] Y. Ma,[47,g] Y. M. Ma,[32] F. E. Maas,[19] M. Maggiora,[74a,74c] S. Malde,[69] Q. A. Malik,[73] A. Mangoni,[29b] Y. J. Mao,[47,g] Z. P. Mao,[1] S. Marcello,[74a,74c] Z. X. Meng,[66] J. G. Messchendorp,[14,64] G. Mezzadri,[30a] H. Miao,[1,63] T. J. Min,[43] R. E. Mitchell,[28] X. H. Mo,[1,58,63] N. Yu. Muchnoi,[5,b] J. Muskalla,[36] Y. Nefedov,[37] F. Nerling,[19,d] I. B. Nikolaev,[5,b] Z. Ning,[1,58] S. Nisar,[12,l] W. D. Niu,[55] Y. Niu,[50] S. L. Olsen,[63] Q. Ouyang,[1,58,63] S. Pacetti,[29b,29c] X. Pan,[55] Y. Pan,[57] A. Pathak,[35] P. Patteri,[29a] Y. P. Pei,[71,58] M. Pelizaeus,[4] H. P. Peng,[71,58] K. Peters,[14,d] J. L. Ping,[42] R. G. Ping,[1,63] S. Plura,[36] S. Pogodin,[37] V. Prasad,[34] F. Z. Qi,[1] H. Qi,[71,58] H. R. Qi,[61] M. Qi,[43] T. Y. Qi,[13,f] S. Qian,[1,58] W. B. Qian,[63] C. F. Qiao,[63] J. J. Qin,[72] L. Q. Qin,[15] X. P. Qin,[13,f] X. S. Qin,[50] Z. H. Qin,[1,58] J. F. Qiu,[1] S. Q. Qu,[61] C. F. Redmer,[36] K. J. Ren,[40] A. Rivetti,[74c] M. Rolo,[74c] G. Rong,[1,63] Ch. Rosner,[19] S. N. Ruan,[44] N. Salone,[45] A. Sarantsev,[37,c] Y. Schelhaas,[36] K. Schoenning,[75] M. Scodeggio,[30a,30b] K. Y. Shan,[13,f] W. Shan,[25] X. Y. Shan,[71,58] J. F. Shangguan,[55] L. G. Shao,[1,63] M. Shao,[71,58] C. P. Shen,[13,f] H. F. Shen,[1,63] W. H. Shen,[63] X. Y. Shen,[1,63] B. A. Shi,[63] H. C. Shi,[71,58] J. L. Shi,[13] J. Y. Shi,[1] Q. Q. Shi,[55] R. S. Shi,[1,63] X. Shi,[1,58] J. J. Song,[20] T. Z. Song,[59] W. M. Song,[35,1] Y. J. Song,[13] Y. X. Song,[47,g] S. Sosio,[74a,74c] S. Spataro,[74a,74c] F. Stieler,[36] Y. J. Su,[63] G. B. Sun,[76] G. X. Sun,[1] H. Sun,[63] H. K. Sun,[1] J. F. Sun,[20] K. Sun,[61] L. Sun,[76] S. S. Sun,[1,63] T. Sun,[1,63] W. Y. Sun,[35] Y. Sun,[10] Y. J. Sun,[71,58] Y. Z. Sun,[1] Z. T. Sun,[50] Y. X. Tan,[71,58] C. J. Tang,[54] G. Y. Tang,[1]

J. Tang,[59] Y. A. Tang,[76] L. Y. Tao,[72] Q. T. Tao,[26,h] M. Tat,[69] J. X. Teng,[71,58] V. Thoren,[75] W. H. Tian,[52] W. H. Tian,[59] Y. Tian,[32,63] Z. F. Tian,[76] I. Uman,[62b] S. J. Wang,[50] B. Wang,[1] B. L. Wang,[63] Bo Wang,[71,58] C. W. Wang,[43] D. Y. Wang,[47,g] F. Wang,[72] H. J. Wang,[39,j,k] H. P. Wang,[1,63] J. P. Wang,[50] K. Wang,[1,58] L. L. Wang,[1] M. Wang,[50] Meng Wang,[1,63] S. Wang,[39,j,k] S. Wang,[13,f] T. Wang,[13,f] T. J. Wang,[44] W. Wang,[72] W. Wang,[59] W. P. Wang,[71,58] X. Wang,[47,g] X. F. Wang,[39,j,k] X. J. Wang,[40] X. L. Wang,[13,f] Y. Wang,[61] Y. D. Wang,[46] Y. F. Wang,[1,58,63] Y. H. Wang,[48] Y. N. Wang,[46] Y. Q. Wang,[1] Yaqian Wang,[18,1] Yi Wang,[61] Z. Wang,[1,58] Z. L. Wang,[72] Z. Y. Wang,[1,63] Ziyi Wang,[63] D. Wei,[70] D. H. Wei,[15] F. Weidner,[68] S. P. Wen,[1] C. W. Wenzel,[4] U. Wiedner,[4] G. Wilkinson,[69] M. Wolke,[75] L. Wollenberg,[4] C. Wu,[40] J. F. Wu,[1,63] L. H. Wu,[1] L. J. Wu,[1,63] X. Wu,[13,f] X. H. Wu,[35] Y. Wu,[71] Y. H. Wu,[55] Y. J. Wu,[32] Z. Wu,[1,58] L. Xia,[71,58] X. M. Xian,[40] T. Xiang,[47,g] D. Xiao,[39,j,k] G. Y. Xiao,[43] S. Y. Xiao,[1] Y. L. Xiao,[13,f] Z. J. Xiao,[42] C. Xie,[43] X. H. Xie,[47,g] Y. Xie,[50] Y. G. Xie,[1,58] Y. H. Xie,[7] Z. P. Xie,[71,58] T. Y. Xing,[1,63] C. F. Xu,[1,63] C. J. Xu,[59] G. F. Xu,[1] H. Y. Xu,[66] Q. J. Xu,[17] Q. N. Xu,[31] W. Xu,[1,63] W. L. Xu,[66] X. P. Xu,[55] Y. C. Xu,[78] Y. Xu,[41] Z. P. Xu,[43] Z. S. Xu,[63] F. Yan,[13,f] L. Yan,[13,f] W. B. Yan,[71,58] W. C. Yan,[81] X. Q. Yan,[1] H. J. Yang,[51,e] H. L. Yang,[35] H. X. Yang,[1] Tao Yang,[1] Y. Yang,[13,f] Y. F. Yang,[44] Y. X. Yang,[1,63] Yifan Yang,[1,63] Z. W. Yang,[39,j,k] Z. P. Yao,[50] M. Ye,[1,58] M. H. Ye,[9] J. H. Yin,[1] Z. Y. You,[59] B. X. Yu,[1,58,63] C. X. Yu,[44] G. Yu,[1,63] J. S. Yu,[26,h] T. Yu,[72] X. D. Yu,[47,g] C. Z. Yuan,[1,63] L. Yuan,[2] S. C. Yuan,[1] X. Q. Yuan,[1] Y. Yuan,[1,63] Z. Y. Yuan,[59] C. X. Yue,[40] A. A. Zafar,[73] F. R. Zeng,[50] X. Zeng,[13,f] Y. Zeng,[26,h] Y. J. Zeng,[1,63] X. Y. Zhai,[35] Y. C. Zhai,[50] Y. H. Zhan,[59] A. Q. Zhang,[1,63] B. L. Zhang,[1,63] B. X. Zhang,[1] D. H. Zhang,[44] G. Y. Zhang,[20] H. Zhang,[71] H. H. Zhang,[59] H. H. Zhang,[35] H. Q. Zhang,[1,58,63] H. Y. Zhang,[1,58] J. Zhang,[81] J. J. Zhang,[52] J. L. Zhang,[21] J. Q. Zhang,[42] J. W. Zhang,[1,58,63] J. X. Zhang,[39,j,k] J. Y. Zhang,[1] J. Z. Zhang,[1,63] Jianyu Zhang,[63] Jiawei Zhang,[1,63] L. M. Zhang,[61] L. Q. Zhang,[59] Lei Zhang,[43] P. Zhang,[1,63] Q. Y. Zhang,[40,81] Shuihan Zhang,[1,63] Shulei Zhang,[26,h] X. D. Zhang,[46] X. M. Zhang,[1] X. Y. Zhang,[50] Xuyan Zhang,[55] Y. Zhang,[69] Y. Zhang,[72] Y. T. Zhang,[81] Y. H. Zhang,[1,58] Yan Zhang,[71,58] Yao Zhang,[1] Z. H. Zhang,[1] Z. L. Zhang,[35] Z. Y. Zhang,[44] Z. Y. Zhang,[76] G. Zhao,[1] J. Zhao,[40] J. Y. Zhao,[1,63] J. Z. Zhao,[1,58] Lei Zhao,[71,58] Ling Zhao,[1] M. G. Zhao,[44] S. J. Zhao,[81] Y. B. Zhao,[1,58] Y. X. Zhao,[32,63] Z. G. Zhao,[71,58] A. Zhemchugov,[37,a] B. Zheng,[72] J. P. Zheng,[1,58] W. J. Zheng,[1,63] Y. H. Zheng,[63] B. Zhong,[42] X. Zhong,[59] H. Zhou,[50] L. P. Zhou,[1,63] X. Zhou,[76] X. K. Zhou,[7] X. R. Zhou,[71,58] X. Y. Zhou,[40] Y. Z. Zhou,[13,f] J. Zhu,[44] K. Zhu,[1] K. J. Zhu,[1,58,63] L. Zhu,[35] L. X. Zhu,[63] S. H. Zhu,[70] S. Q. Zhu,[43] T. J. Zhu,[13,f] W. J. Zhu,[13,f] Y. C. Zhu,[71,58] Z. A. Zhu,[1,63] J. H. Zou,[1] and J. Zu[71,58]

(BESIII Collaboration)

[1]*Institute of High Energy Physics, Beijing 100049, People's Republic of China*
[2]*Beihang University, Beijing 100191, People's Republic of China*
[3]*Beijing Institute of Petrochemical Technology, Beijing 102617, People's Republic of China*
[4]*Bochum Ruhr-University, D-44780 Bochum, Germany*
[5]*Budker Institute of Nuclear Physics SB RAS (BINP), Novosibirsk 630090, Russia*
[6]*Carnegie Mellon University, Pittsburgh, Pennsylvania 15213, USA*
[7]*Central China Normal University, Wuhan 430079, People's Republic of China*
[8]*Central South University, Changsha 410083, People's Republic of China*
[9]*China Center of Advanced Science and Technology, Beijing 100190, People's Republic of China*
[10]*China University of Geosciences, Wuhan 430074, People's Republic of China*
[11]*Chung-Ang University, Seoul 06974, Republic of Korea*
[12]*COMSATS University Islamabad, Lahore Campus, Defence Road, Off Raiwind Road, 54000 Lahore, Pakistan*
[13]*Fudan University, Shanghai 200433, People's Republic of China*
[14]*GSI Helmholtzcentre for Heavy Ion Research GmbH, D-64291 Darmstadt, Germany*
[15]*Guangxi Normal University, Guilin 541004, People's Republic of China*
[16]*Guangxi University, Nanning 530004, People's Republic of China*
[17]*Hangzhou Normal University, Hangzhou 310036, People's Republic of China*
[18]*Hebei University, Baoding 071002, People's Republic of China*
[19]*Helmholtz Institute Mainz, Staudinger Weg 18, D-55099 Mainz, Germany*
[20]*Henan Normal University, Xinxiang 453007, People's Republic of China*
[21]*Henan University, Kaifeng 475004, People's Republic of China*
[22]*Henan University of Science and Technology, Luoyang 471003, People's Republic of China*
[23]*Henan University of Technology, Zhengzhou 450001, People's Republic of China*
[24]*Huangshan College, Huangshan 245000, People's Republic of China*
[25]*Hunan Normal University, Changsha 410081, People's Republic of China*

[26]*Hunan University, Changsha 410082, People's Republic of China*
[27]*Indian Institute of Technology Madras, Chennai 600036, India*
[28]*Indiana University, Bloomington, Indiana 47405, USA*
[29a]*INFN Laboratori Nazionali di Frascati, INFN Laboratori Nazionali di Frascati, I-00044 Frascati, Italy*
[29b]*INFN Sezione di Perugia, I-06100 Perugia, Italy*
[29c]*University of Perugia, I-06100 Perugia, Italy*
[30a]*INFN Sezione di Ferrara, INFN Sezione di Ferrara, I-44122 Ferrara, Italy*
[30b]*University of Ferrara, I-44122 Ferrara, Italy*
[31]*Inner Mongolia University, Hohhot 010021, People's Republic of China*
[32]*Institute of Modern Physics, Lanzhou 730000, People's Republic of China*
[33]*Institute of Physics and Technology, Peace Avenue 54B, Ulaanbaatar 13330, Mongolia*
[34]*Instituto de Alta Investigación, Universidad de Tarapacá, Casilla 7D, Arica 1000000, Chile*
[35]*Jilin University, Changchun 130012, People's Republic of China*
[36]*Johannes Gutenberg University of Mainz, Johann-Joachim-Becher-Weg 45, D-55099 Mainz, Germany*
[37]*Joint Institute for Nuclear Research, 141980 Dubna, Moscow region, Russia*
[38]*Justus-Liebig-Universitaet Giessen, II. Physikalisches Institut, Heinrich-Buff-Ring 16, D-35392 Giessen, Germany*
[39]*Lanzhou University, Lanzhou 730000, People's Republic of China*
[40]*Liaoning Normal University, Dalian 116029, People's Republic of China*
[41]*Liaoning University, Shenyang 110036, People's Republic of China*
[42]*Nanjing Normal University, Nanjing 210023, People's Republic of China*
[43]*Nanjing University, Nanjing 210093, People's Republic of China*
[44]*Nankai University, Tianjin 300071, People's Republic of China*
[45]*National Centre for Nuclear Research, Warsaw 02-093, Poland*
[46]*North China Electric Power University, Beijing 102206, People's Republic of China*
[47]*Peking University, Beijing 100871, People's Republic of China*
[48]*Qufu Normal University, Qufu 273165, People's Republic of China*
[49]*Shandong Normal University, Jinan 250014, People's Republic of China*
[50]*Shandong University, Jinan 250100, People's Republic of China*
[51]*Shanghai Jiao Tong University, Shanghai 200240, People's Republic of China*
[52]*Shanxi Normal University, Linfen 041004, People's Republic of China*
[53]*Shanxi University, Taiyuan 030006, People's Republic of China*
[54]*Sichuan University, Chengdu 610064, People's Republic of China*
[55]*Soochow University, Suzhou 215006, People's Republic of China*
[56]*South China Normal University, Guangzhou 510006, People's Republic of China*
[57]*Southeast University, Nanjing 211100, People's Republic of China*
[58]*State Key Laboratory of Particle Detection and Electronics, Beijing 100049, Hefei 230026, People's Republic of China*
[59]*Sun Yat-Sen University, Guangzhou 510275, People's Republic of China*
[60]*Suranaree University of Technology, University Avenue 111, Nakhon Ratchasima 30000, Thailand*
[61]*Tsinghua University, Beijing 100084, People's Republic of China*
[62a]*Turkish Accelerator Center Particle Factory Group, Istinye University, 34010 Istanbul, Turkey*
[62b]*Near East University, Nicosia, North Cyprus 99138, Mersin 10, Turkey*
[63]*University of Chinese Academy of Sciences, Beijing 100049, People's Republic of China*
[64]*University of Groningen, NL-9747 AA Groningen, The Netherlands*
[65]*University of Hawaii, Honolulu, Hawaii 96822, USA*
[66]*University of Jinan, Jinan 250022, People's Republic of China*
[67]*University of Manchester, Oxford Road, Manchester M13 9PL, United Kingdom*
[68]*University of Muenster, Wilhelm-Klemm-Strasse 9, 48149 Muenster, Germany*
[69]*University of Oxford, Keble Road, Oxford OX13RH, United Kingdom*
[70]*University of Science and Technology Liaoning, Anshan 114051, People's Republic of China*
[71]*University of Science and Technology of China, Hefei 230026, People's Republic of China*
[72]*University of South China, Hengyang 421001, People's Republic of China*
[73]*University of the Punjab, Lahore-54590, Pakistan*
[74a]*University of Turin and INFN, University of Turin, I-10125 Turin, Italy*
[74b]*University of Eastern Piedmont, I-15121 Alessandria, Italy*
[74c]*INFN, I-10125 Turin, Italy*
[75]*Uppsala University, Box 516, SE-75120 Uppsala, Sweden*
[76]*Wuhan University, Wuhan 430072, People's Republic of China*
[77]*Xinyang Normal University, Xinyang 464000, People's Republic of China*
[78]*Yantai University, Yantai 264005, People's Republic of China*

[79]*Yunnan University, Kunming 650500, People's Republic of China*
[80]*Zhejiang University, Hangzhou 310027, People's Republic of China*
[81]*Zhengzhou University, Zhengzhou 450001, People's Republic of China*

[a]Also at the Moscow Institute of Physics and echnology, Moscow 141700, Russia.
[b]Also at the Novosibirsk State University, Novosibirsk 630090, Russia.
[c]Also at the NRC "Kurchatov Institute", PNPI, 188300 Gatchina, Russia.
[d]Also at Goethe University Frankfurt, 60323 Frankfurt am Main, Germany.
[e]Also at Key Laboratory for Particle Physics, Astrophysics and Cosmology, Ministry of Education; Shanghai Key Laboratory for Particle Physics and Cosmology; Institute of Nuclear and Particle Physics, Shanghai 200240, People's Republic of China.
[f]Also at Key Laboratory of Nuclear Physics and Ion-beam Application (MOE) and Institute of Modern Physics, Fudan University, Shanghai 200443, People's Republic of China.
[g]Also at State Key Laboratory of Nuclear Physics and Technology, Peking University, Beijing 100871, People's Republic of China.
[h]Also at School of Physics and Electronics, Hunan University, Changsha 410082, China.
[i]Also at Guangdong Provincial Key Laboratory of Nuclear Science, Institute of Quantum Matter, South China Normal University, Guangzhou 510006, China.
[j]Also at Frontiers Science Center for Rare Isotopes, Lanzhou University, Lanzhou 730000, People's Republic of China.
[k]Also at Lanzhou Center for Theoretical Physics, Lanzhou University, Lanzhou 730000, People's Republic of China.
[l]Also at the Department of Mathematical Sciences, IBA, Karachi 75270, Pakistan.